Myocardial Perfusion Characterization From Contrast Angiography Spectral Distribution

Debora Gil*, Oriol Rodriguez-Leor, Petia Radeva, and Josepa Mauri

Abstract—Despite recovering a normal coronary flow after acute myocardial infarction, percutaneous coronary intervention does not guarantee a proper perfusion (irrigation) of the infarcted area. This damage in microcirculation integrity may detrimentally affect the patient survival. Visual assessment of the myocardium opacification in contrast angiography serves to define a subjective score of the microcirculation integrity myocardial blush analysis (MBA). Although MBA correlates with patient prognosis its visual assessment is a very difficult task that requires of a highly expertise training in order to achieve a good intraobserver and interobserver agreement. In this paper, we provide objective descriptors of the myocardium staining pattern by analyzing the spectrum of the image local statistics. The descriptors proposed discriminate among the different phenomena observed in the angiographic sequence and allow defining an objective score of the myocardial perfusion.

Index Terms—Contrast angiography, myocardial perfusion, spectral analysis.

I. INTRODUCTION

PRIMARY angioplasty is the usual way to treat acute myocardial infarction as it restores a normal flow of the occluded artery. However, recovering a proper coronary flow after primary angioplasty does not always correlate with an adequate irrigation (myocardial perfusion) of the area subtended by the artery [1]. A deficient perfusion affects the patient survival and its assessment has been a main concern in recent clinical research ([2]–[11]).

Visual assessment of the contrast opacification of the myocardial area subtended by the infarcted vessel in coronary angiographies allows defining a subjective score (the myocardial blush grade [3], [4]) of the microvascular function. Several clinical studies select the myocardial blush grade as an efficient prognosis tool ([5]–[7]). It correlates with ST-segment elevation index and an integrated analysis of both parameters allows an accurate assessment of myocardial perfusion [5]. It is one of the best parameters for assessment of the left ventricular function recovery [6]. Therefore, it is a good predictor for long-term mortality after angioplasty [7].

*D. Gil is with the Computer Vision Center, Edifici O, Universitat Autònoma de Barcelona, 08193 Bellaterra, Spain (e-mail: debora@cvc.uab.es).

P. Radeva is with the Computer Vision Center, Edifici O, Universitat Autònoma de Barcelona, 08193 Bellaterra, Spain (e-mail: debora@cvc.uab.es).

O. Rodriguez-Leor and J. Mauri are with the Hospital Universitari "Germans Trias i Pujol," 08916 Badalona, Spain.
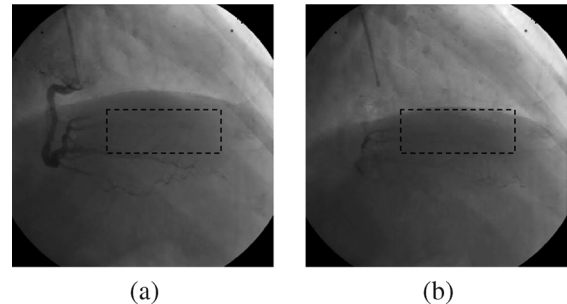
Fig. 1. Myocardial staining in contrast angiography: (a) beginning of microcirculation staining and (b) maximum microcirculation staining.

Myocardial staining in contrast angiography is a faint phenomenon difficult to appreciate by its low signal-to-noise ratio, as the images in Fig. 1 illustrate. The angiography in Fig. 1(a) captures the beginning of the microcirculation staining and the angiography in Fig. 1(b) its maximum opacification. The microcirculation absorption region corresponds to the dashed squares, which hardly present any difference in their grey-levels intensity. It follows that determination of the blush grade might suffer from a significant interobserver variability in the case of nonexperienced observers [8]. This fact questions its reliability [9] and it is a major limitation for a systematic application in clinical studies. By the relatively novelty of the technique, there are few techniques addressing objective quantification of the myocardial microcirculation.

Up to our knowledge, the available strategies for quantitative myocardial blush analysis (MBA) assessment [10], [11] still require a substantial manual intervention and, thus, are subject to high interobserver variability. The methodology described in [10] uses digital image subtraction to remove nonstaining phenomena and proposes grey-level differences between initial and final angiography frames to quantify of myocardial perfusion. Although they report high correlation to manually determined perfusion grades, it has some technical limitations. On one hand, subtraction requires synchronization with cardiac cycle and the patient in apnea to avoid breathing interference. On the other hand, it is not guaranteed that the selected first and last angiographic planes capture the minimum and maximum staining. The most recent strategy in [11] relies on absorption velocities but it also requires accurate identification of the initial and final staining times.

In this paper, we approach the objective determination of the myocardial staining pattern in contrast angiography from an image processing point of view. We focus on two main issues: reliable extraction of the staining pattern and objective measurement of the myocardial perfusion.

Contrast angiographic sequences show different phenomena: breathing, heart beating, arterial staining, myocardial staining,
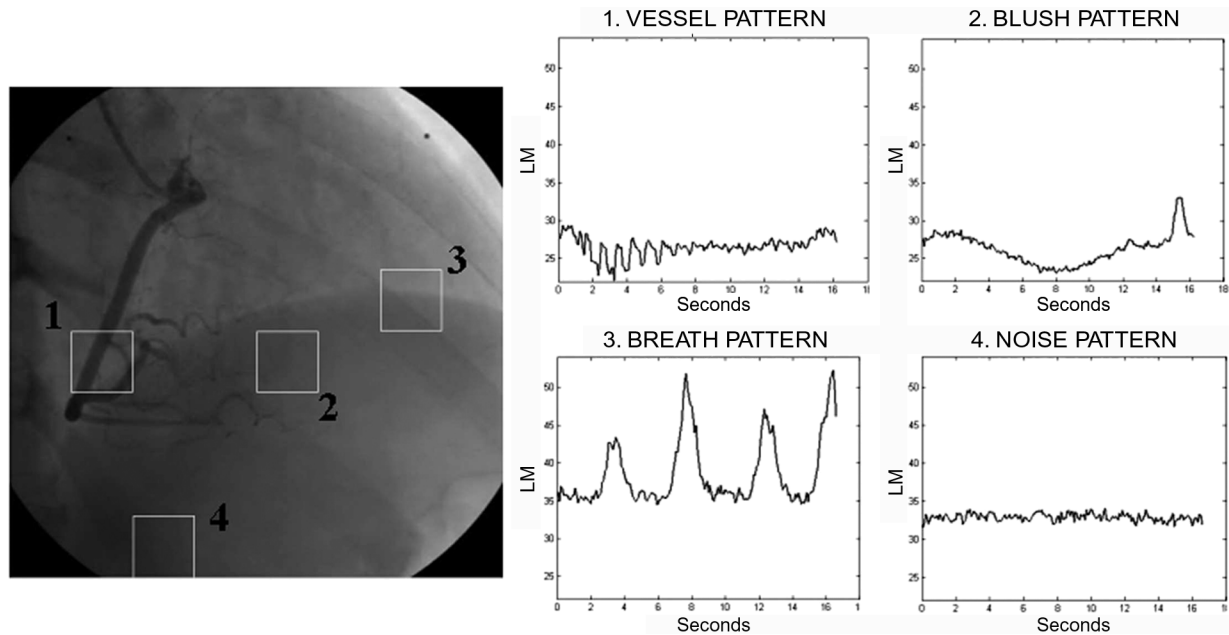
Fig. 2. Patterns for the different areas. 1: Arterial staining. 2: Myocardial staining. 3: Breathing. 4: Noise.

and radiological noise. The first two phenomena are major disturbance in the myocardial blush grade determination [12] and force, up to this moment, recording sequences with the patient performing a breath-hold. Statistical analysis of the Fourier spectrum [13] of the evolution in time of the image grey-level local average allows identifying each of the above events. The Fourier coefficient of the first frequency provides a reliable extraction of the myocardium staining pattern regardless of breath holding. We introduce a novel objective measure of the myocardial perfusion [the perfusion staining ratio (PSR)] defined in terms of the ratio between arterial and myocardial staining. We also provide a methodology for a semiautomatic computation from contrast angiography sequences.

Our experiments systematically explore the performance and limitations of the staining patterns and the PSR extraction. We have also explored PSR applicability in clinical practice and show that the probability density function of PSR in healthy people significantly differs from the distribution obtained from infarcted patients.

The paper is organized as follows. In Section II, we describe the myocardial staining feature space and define the PSR. Sections III and IV-A are devoted to the assessment of the extraction of the staining patterns and the computation of the index. Section IV-B shows the applicability of PSR for myocardium microvascular function determination. Finally, Section VI exposes discussions and further lines of research.

II. PERFUSION CHARACTERIZATION

A. Staining Space

The microcirculation contrast absorption can be detected by changes in the image grey-values along an angiographic sequence [10]. In order to minimize the impact of radiologic noise we consider the image local mean computed in sliding windows of 32×32 pixels. The variation in the baseline luminosity of images along the sequence distorts the evolution pattern of grey-values. This motivates normalizing image grey values before computing the local mean

$$ImN(x,y) = \frac{Im(x,y) - \mu(Im)}{\sigma(Im)}$$

where $\mu(Im)$ is the image mean and $\sigma(Im)$ its standard deviation. The values of the local mean of ImN for all frames provides each pixel with a function, namely LM, that describes the average contrast absorbed by the tissue along time.

Fig. 2 shows the LM patterns obtained at the white squares on the angiography shown on the left side of the image. The angiography is a projection of the right coronary artery, which is located on the left side of the image. The myocardial area subtended by the artery is the region with small branches on the right-hand side of the artery. The projection also shows the diaphragm as a horizontal border splitting the image in two half planes of different baseline luminosity. We have chosen four representative areas: arterial staining (number 1), myocardial staining at an area not swept by the diaphragm border (number 2), diaphragm movement reflecting breathing (number 3), and pure background radiological noise (number 4). The plots obtained for stained areas present a local minimum at the time the maximum contrast opacification is achieved. The artery periodic movement due to heart beating is reflected by oscillations in the LM pattern during the vessel opacification phase. The diaphragm rhythmic movement also introduces an oscillation in the grey-level average with a frequency equal to the breathing one.

The myocardial staining shown in Fig. 2 is an ideal pattern free from any physiological phenomena interference. In the general case, the signal obtained (solid line in Fig. 3) is the contribution of four main phenomena: breathing, heart beating, myocardial dyeing, and noise. The first two, especially breathing, are main artifacts that might distort the staining pattern [12]. Each phenomenon has a distinctive repetition pattern (frequency) and, thus, the Fourier development [13] of LM decouples them. The
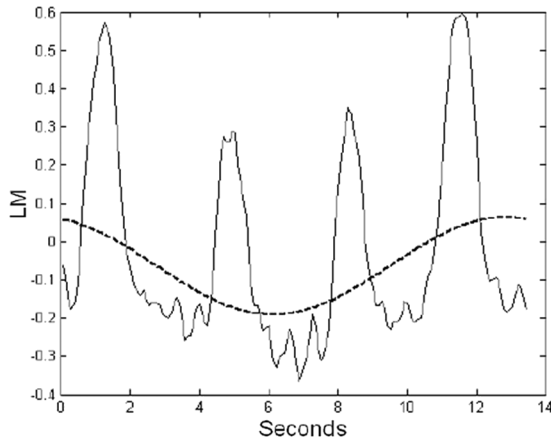
Fig. 3. Extraction of the myocardial staining pattern (dashed line) from LM signal (solid line).

frequency range is learned by supervised classification of the spectrum of a training set of signals. For each patient, three different sequences were recorded.

1) A sequence without contrast injection and the patient normally breathing in order to learn diaphragm movements and background noise.
2) A sequence with contrast injection and the patient holding breathing for learning the frequency range of heart beating and myocardial staining.
3) A test sequence with contrast injection and the patient normally breathing.

The amplitudes of the spectrum of the LM patterns define a probability density function (pdf) in the frequency domain, which we model with a mixture of Gaussians [14]. The Bayes classifier for the four classes gives [15] the following frequency ranges for the physiological phenomena. Myocardial staining is below 10 repetitions per minute, breathing is in the range (10, 45) repetitions per minute, heart beating is within (45, 200) repetitions and any frequency above 200 repetitions corresponds to radiological noise. For each frequency range, the frequency of maximum amplitude is the main descriptor of the phenomenon.

In the case of myocardial staining, since it is a phenomenon that happens only once, for each contrast injection, it is given by the first frequency of LM Fourier development. Fig. 3 shows the differences between the original LM signal (solid line) and the staining pattern (dashed line). We note that breathing movements mainly contribute in the LM profile, which hides the weak staining pattern underneath.

The descriptors we propose to characterize staining are the amplitude and phase of the Fourier coefficient of the first frequency. The amplitude represents the maximum staining and will be noted by $I_{\max}$. The phase corresponds to the time (given in either seconds or number of frames) such maximum is achieved and will be noted by $t_{I_{\max}}$. These staining descriptors constitute what we call the staining space.

B. PSR

The set of descriptors differentiates three different areas on the angiography: arterial staining (A), myocardial staining (M), and area without staining (N). The three classes are well distinguished in the scattered plot given by the values $(I_{\max}, t_{I_{\max}})$, as

(a)
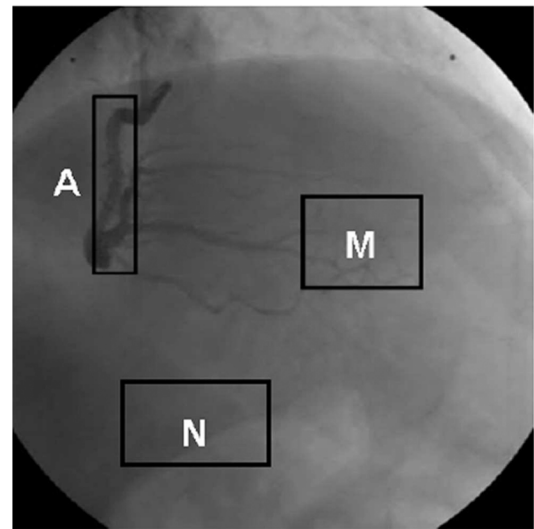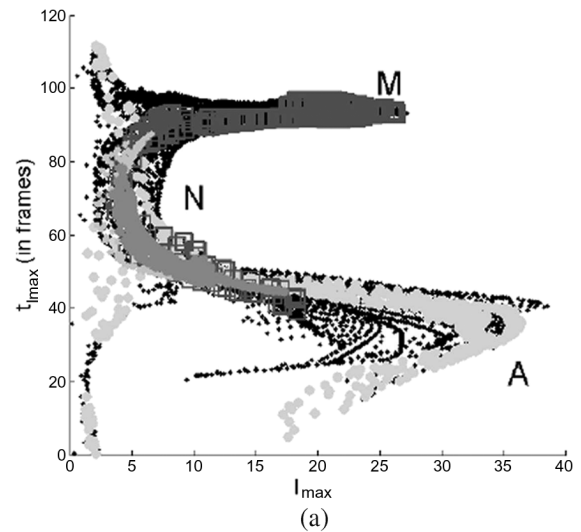
(b)

Fig. 4. Different staining phenomena detected: (a) perfusion feature space and (b) angiography used to extract characteristics.

illustrated in Fig. 4(a). The feature space given on Fig. 4(a) represents the maximum intensity $I_{\max}$ on the x axis and the time $t_{I_{\max}}$ in frames on the y axis. Each class is shown in a different grey intensity: light for arterial staining (labelled A), dark for myocardial staining (labelled M), and medium for background noise (labelled N). The areas used to compute the descriptors are enclosed in squares with the same labels on the angiography shown in Fig. 4(b).

Every staining phenomenon observed in the angiography introduces an intensity (horizontal) peak in the staining space scattered plots. In an ideal setting, scatter plots have a tilted U-shape with two prominent horizontal arms [labelled A and M in Fig. 4(a)] leaning on a layer of background noise pixels [labelled N in Fig. 4(a)]. The first arm in time (A) represents epicardial arterial flow and the second one (M) microcirculation contrast absorption. The extreme of each of the arms corresponds to the points achieving the maximum staining of the vessel and myocardium. Their vertical separation is the time the myocardium takes to absorb contrast (and, thus, blood). In the usual case, we might find a third peak corresponding to either

branches staining, vessel contrast drainage, or aortic contrast flow-out. The latter, which we call flashing, is a main artifact since it is prone to be confused with the arterial staining peak.

In noninfarcted subjects, the average contrast flowing through the artery is equal to the average contrast absorbed by tissue. In fact, the myocardial peak intensity decreases in the measure that either the main artery or the microcirculation are obstructed. We define our PSR as

$$\mathrm{PSR} = \min\left(\frac{\mu(M)}{\mu(A)}, \frac{\mu(A)}{\mu(M)}\right) \qquad (1)$$

for $\mu(A)$ and $\mu(M)$ the average arterial and myocardial staining. The above definition ensures that PSR is a quantity in the range [0,1]. The lower bound of PSR (achieved in the case that $\mu(M) = 0$) indicates a lack of microvascular function, while the closer to one PSR is the better perfusion we have on the area irrigated by the main artery.

Averages in (1) are computed as the trimmed mean [16] of $I_{\max}$ intensity values for pixels on the main coronary artery and its irrigated territory. In our case, the trimmed mean is the average of intensity values obtained discarding sample distribution queues of the 10% percentile each.

C. PSR Computation

Computation of the ratio PSR requires identification of the artery and myocardium staining points in either the angiography or the staining space. In any case, the percentage of background points involved in the computation of trimmed means should be as small as possible. Since the staining agent does not opacify background pixels, their maximum staining is significantly lower than the one achieved at arterial and perfusion areas. We use a two-class clustering [14] of the $I_{\max}$ values to discriminate staining peaks from low staining points. The cluster achieving the maximum $I_{\max}$ value contains the staining peaks. The minimum value of $I_{\max}$ on such cluster is a lower threshold Th_N for staining points. Staining peaks are given by points with $I_{\max}$ above Th_N. From now on, we will only consider such points, which will be referred to as staining points. We separate myocardial and arterial staining peaks as follows.

Manual Myocardial Peak Identification. On one hand, myocardial pixel appearance in the staining space is strongly influenced by the microcirculation integrity. The prominence of the staining peak ranges from a size comparable to the arterial peak, in the case of healthy and MBG3 coronary arteries, down to confusing with background pixels intensity in the case of infarcted and MBG0 arteries. Such variability is prone to mislead automated procedures for myocardial peak identification in the staining space.

On the other hand, the location of the region of interest on the angiography might substantially vary among cases. Given that visual identification of the myocardial bed irrigated by the infarcted artery is a routine task, the perfusion area is manually traced on the angiography.

Myocardial staining points are those pixels inside the region of interest presenting a maximum intensity above Th_N.

Automatic Arterial Peak Identification. Discarding myocardial staining points, the remaining staining points contain arterial pixels as well as other remarkable staining phenomena, such as secondary branches staining and aortic flashing. The latter is a main artifact, normally synchronized with arterial staining, prone to deviate averages. We propose the following strategy for automatically detecting arterial staining points.

We note that the opacified artery looks like a valley on the angiography, while aortic flashing presents a uniform intensity appearance concentrated around the ostium. Consequently, the aortic flashing maximum intensity is significantly higher than the arterial one. We consider that points with a $I_{\max}$ below a given value, namely Th_A, belong to the main coronary artery. In order to define Th_A we proceed as follows.

Let $\mathcal{I}$ be the random variable given by the intensity values $I_{\max}$ at staining points outside the myocardial region of interest. By the appearance on the angiography, its probability density function decomposes into a Gaussian-like distribution (arterial points) and a uniform distribution (remaining pixels). The threshold Th_A is the value best splitting the former distributions.

A Gaussian and a uniform distribution have different convexity profiles. This fact is reflected in their kurtosis, which is zero for a Gaussian distribution and negative for a uniform one. For each intensity value i let us define the kurtosis γ^{+i} of the $I_{\max}$ values above i as

$$\gamma^{+i} = \frac{n\sum_{k=1}^{k=n}\left(\mathcal{I}_k^{i+} - \overline{\mathcal{I}}^{i+}\right)^4}{\left(\sum_{k=1}^{k=n}\left(\mathcal{I}_k^{i+} - \overline{\mathcal{I}}^{i+}\right)^2\right)^2} - 3$$

for $(\mathcal{I}_k^{i+})_{k=1:n}$ all samples above the intensity i and $\overline{\mathcal{I}}^{i+} = \sum_{k=1}^{k=n}\mathcal{I}_k^{i+}$ the sample mean. The threshold Th_A is given by the first local minimum of γ^{+i}, since such value ensures the most uniformity of the distribution on its right-hand side.

The arterial staining points are those pixels not belonging to the myocardial peak, which intensity $I_{\max}$ is in the range $[Th_N, Th_A]$.

Fig. 5 illustrates the main steps for the computation of arterial and myocardial staining peaks. The plot in Fig. 5(a) shows the staining space with the myocardial staining points (labelled M) and the arterial ones (labelled A). The arterial peak presents a significant aortic flashing which enlarges the range of its intensity values. Vertical lines indicate the intensity thresholds: the solid grey line marks the threshold (Th_N) separating staining peaks from noise and the dashed black one marks the threshold (Th_A) separating arterial staining from aortic flashing. The set of points in grey on the "M" peak correspond to the region in black on the angiography shown in Fig. 5(b). In this case, the region contains background points with a low staining, which lie below Th_N on the staining space plot. The probability density function of $\mathcal{I}$ is shown in the histogram of Fig. 5(c). The threshold Th_A is represented with a dashed line and defines the arterial points shown in grey on the staining space.
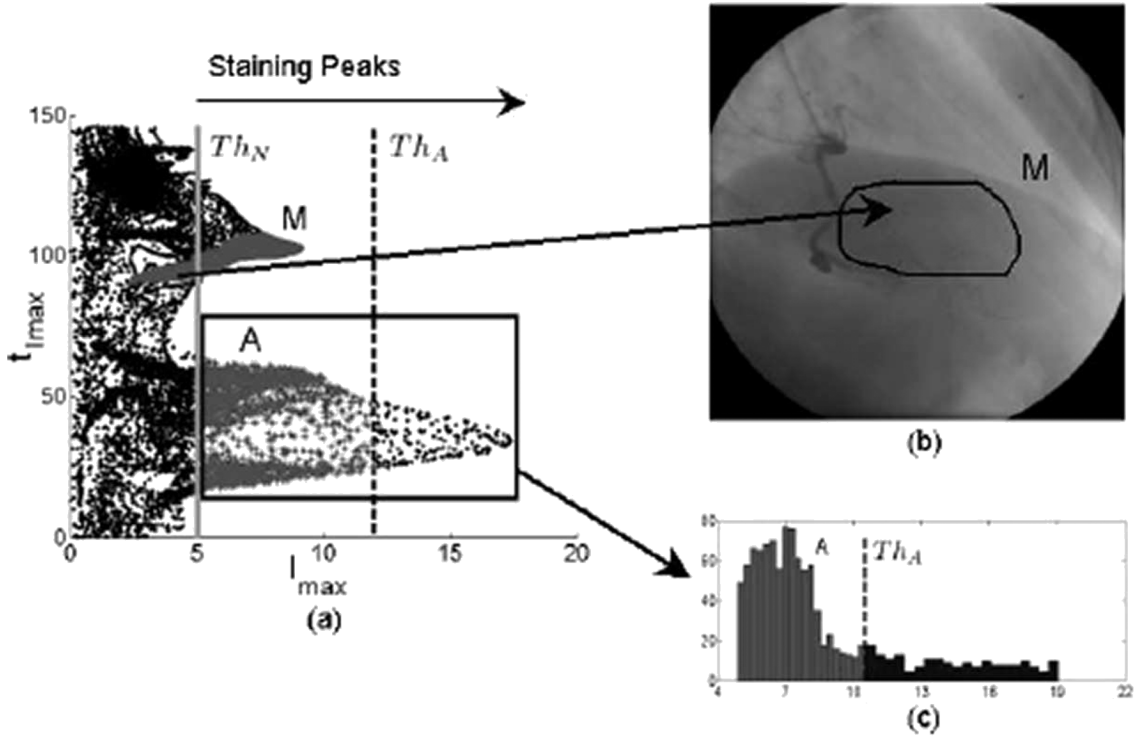
Fig. 5. Main steps involved in the computation of the arterial and myocardial staining points. (a) Selection of arterial (A) and myocardial (M) staining peaks. (b) Manual selection of myocardial points on angiography. (c) Automatic selection of arterial points based on $\mathcal{I}$ Kurtosis.

III. EXPERIMENTAL SETUP

We have analyzed healthy right coronary and anterior descending arteries. The sequences are clinical cases from the Hospital Universitari "Germans Trias i Pujol" in Badalona, Spain. Angiographies have been recorded in DICOM format at 12.5 frames per second. The recording was done exhausting the acquisition time in order to guarantee that the staining agent is completely absorbed by the microcirculation. Panning of the patient table was not allowed during acquisition.

Our experiments have been designed to address the following issues.

A. Staining Pattern Assessment

Since radiological background noise and breathing movements are the main staining artifacts observed in angiographies, experiments focus on determining the influence of the following.

1) *Noise Impact*. We have explored whether the staining curves extracted from the artery and the myocardium are due to contrast opacification or result from radiological artifacts. In order to check the above condition it suffices to show that the patterns obtained at the myocardium are distinct from those extracted from background pixels. This requirement is fulfilled if the proposed descriptors discriminate, for each patient, among the three main classes: arterial dyeing (A), myocardial dyeing (M), and noise (N).

2) *Breath Impact*. Patients breathing is a main interferer with contrast staining and forces taking the sequences with the breath-hold. In order to determine the influence of breathing on the staining patterns, we have compared the classification performance in sequences obtained in apnea and with the patient breathing normally.

We have addressed the above topics by analyzing 23 right coronary arteries without any observable lesion in the angiography with sequences obtained in apnea and with the subject normally breathing. The angulation used to acquire angiographies was right anterior oblique 30 cranial 15 (RAO 30, CRAN 15).

The discriminating capability of the descriptors has been assessed by cross validation [17] on each patient. Cross validation consists in training a classifier with a random sampling of each class and using the remaining pixels as test set. The classifier used was the k-nearest neighbors (k-NN) [14] and the training set was a uniform sampling representing 25% of the pixels. The manual labelling of image pixels was done as follows. The myocardial blush area was manually traced by a clinical expert. The area swept by the right coronary artery and its main branches during the sequence was labelled as arterial staining. The remaining pixels were considered background noise.

The classification error, the precision, the recall and the specificity [14] are the measures we have chosen to assess the discriminating rate of the descriptors. The classification error is the percentage of pixels incorrectly classified. The remaining measures are given in terms of false and true positives (FP, TP) and false and true negatives (FN, TN) as follows:

$$\text{recall} = \frac{\text{TP}}{\text{TP} + \text{FN}} \cdot 100\%$$

$$\text{specificity} = \frac{\text{TN}}{\text{TN} + \text{FP}} \cdot 100\%$$

$$\text{precision} = \frac{\text{TP}}{\text{TP} + \text{FP}} \cdot 100\%.$$
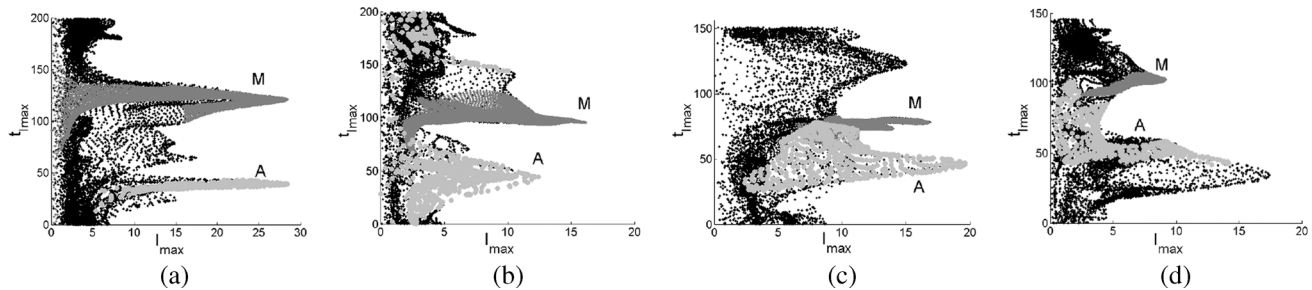
Fig. 6. Staining space variability. (a) Extra staining peak in the middle of the U-shape due to staining of secondary branches, (b) overlapping of arterial and myocardial staining, (c) extra peak at the end of U-shape in the presence of vessel drainage, and (d) enlargement of first peak because of aortic flashing.

TABLE I
CLASSIFICATION ERROR (%) FOR MYOCARDIAL STAINING (M)

APNEA

A in M	N in M	Recall	Specificity	Precision
1.5 ± 1.5	0.8 ± 1.3	97.7 ± 2.3	98.7 ± 0.9	98.0 ± 1.4

BREATH

A in M	N in M	Recall	Specificity	Precision
1.1 ± 0.9	0.7 ± 0.9	98.2 ± 1.7	98.5 ± 0.9	97.8 ± 1.3

Recall corresponds to the positive detection rate, specificity is the negative detection rate, and precision indicates the percentage of noise (negative cases) included in the samples detected as positive ones. In our case, the positive case is the class of interest and the negative one the remaining two classes.

For all measures, we report the error range given by the mean $\pm$ standard deviation computed for the 23 patients under study. Regarding differences between results obtained for patients in apnea and normally breathing, t-student tests are used to detect any significant difference between the mean of classification errors.

B. PSR Assessment

Given that the extracted staining patterns correctly represent contrast absorption, the proposed PSR index is suitable for clinical application provided that we check the following.

1) *PSR Computation Accuracy*. Straight comparison between PSR values computed using automatic and manually selected points reflects PSR accuracy.
2) *PSR Computation Reliability*. In order to ensure that $\mu(A)$ has been computed from arterial points, we must check the accuracy of their automated selection.

By their different arterial dynamics we have added 16 left anterior descending arteries without any observable lesion in the angiography to the set of right coronary arteries used to validate staining patterns. The projection used for the left anterior descending was the left oblique anterior 90 (LAO 90) in order to ensure that there is no overlapping between the left anterior descending and the circumflex beds.

For PSR accuracy assessment, we have chosen regression analysis in order to compare manual and automatically computed values. Concerning PSR reliability, we report the precision ranges of the selected arterial points.

IV. RESULTS

A. Staining Pattern Assessment

Fig. 6 illustrates the qualitative and quantitative variability of the staining space appearance. Arterial pixels (labelled A)

are shown in light grey and myocardial ones (labelled M) in dark grey. Even for healthy people, there is a large variability in U-shape parameters and, in general, in the staining space appearance. Average staining intensities depend, among other factors, on the overlapping of structures on the projection plane, as well as on the density of the organs surrounding the myocardium. The vertical temporal delay between staining peaks mainly depends on the amount of contrast injected per time unit, the cardiac frequency, and the microvascular integrity. Regarding the staining space configuration, vessel phase, staining of secondary branches and the aortic flashing introduce a third peak of variable temporal position. Fig. 6(a) shows the usual U-shape with a small peak between arterial and myocardial peaks due to secondary branches. In Fig. 6(b), there is a substantial reduction in the time gap between arterial and myocardium staining. Fig. 6(c) shows the vessel phase appearing as a third peak at the end of the sequence. Finally, Fig. 6(d) presents a significant aortic flash at the beginning of the sequence and almost synchronized with arterial staining.

Tables I–III summarize the classification error in percentage for each of the classes. Table I gives errors for myocardial staining with the label "A in M" for pixels identified as artery and "N in M" for pixels classified as noise. Table II gives the errors for arterial staining with the label "M in A" for pixels classified as myocardial staining and "N in A" for pixels classified as noise. Finally, Table III contains errors for the background class with "M in N" standing for pixels classified as myocardial staining and "A in N" for pixels classified as artery. In all tables, the last three columns report recall, specificity, and precision.

The statistical ranges given in Table I select myocardial staining as the best characterized phenomena. It achieves an optimal detection rate with a recall over 95% and a precision over 96%. Besides, it presents a low sensitivity to noise, since the percentage of background pixels having a myocardial staining pattern is under 5% (100%—specificity in Table III). The error percentages "N in A" in Table II and "A in N" in Table III indicate that the descriptors capability for discrimi-

TABLE II
CLASSIFICATION ERROR (%) FOR ARTERIAL STAINING (A)

APNEA

M in A	N in A	Recall	Specificity	Precision
1.8 ± 1.6	6.6 ± 1.9	91.2 ± 2.7	95.2 ± 1.8	91.6 ± 4.7

BREATH

M in A	N in A	Recall	Specificity	Precision
1.9 ± 1.6	6.6 ± 3.3	91.6 ± 3.5	96.8 ± 2.2	91.9 ± 6.3

TABLE III
CLASSIFICATION ERROR (%) FOR BACKGROUND NOISE (N)

APNEA

M in N	A in N	Recall	Specificity	Precision
0.7 ± 0.5	6.6 ± 2.4	93.1 ± 2.5	96.6 ± 1.3	92.8 ± 3.5

BREATH

M in N	A in N	Recall	Specificity	Precision
0.5 ± 0.7	6.2 ± 4.3	93.4 ± 4.2	97.4 ± 1.4	93.8 ± 4.1

TABLE IV
APNEA VERSUS BREATHING. STUDENT t-TEST STATISTICAL SUMMARY

	p-value	Confidence Interval
'A in M'	0.0695	$(-0.0168, 0.0036)$
'N in M'	0.1941	$(-0.0220, 0.0009)$
'M in A'	0.6843	$(-0.0237, 0.0352)$
'N in A'	0.8006	$(-0.0235, 0.0302)$
'M in N'	0.2029	$(-0.0339, 0.0078)$
'A in N'	0.9445	$(-0.0238, 0.0222)$

nating arterial staining from background noise decreases. Still we have a detection rate (given by the recall and precision in Table II) above 85.6%. This increase in error is due to a difficult manual identification of arterial pixels and it is discussed in detail in Section VI.

Concerning breath impact, we have compared separately the six classification errors. According to a Kolmogorov–Smirnov goodness-of-fit test there is no evidence of nonnormality in classification errors ($p > 0.1$). Therefore, we use a student t-test for pairwise data to compare errors obtained in apnea and breathing. The null hypothesis is on the mean of the difference between breathing and apnea errors. Table IV shows the p-values and confidence intervals (CI) for the mean of the difference at significant level $\alpha = 0.05$. None of the tests are significant enough ($p > 0.0695$) as to reject equal error means. The confidence interval for the errors "A in M," "N in M," and "M in N" are not centered in zero, but negative biased. This indicates that errors tend to be lower in the case of sequences taken with the patient normally breathing. As for the remaining classification errors, there is no evidence of bias with, at most, a $\pm 3\%$ of difference.

B. PSR Assessment

Figs. 7 and 8 show the regression between manual (x axis) and semi-automatically computed PSR (y axis). Plots in Fig. 7 are for the 23 right coronary arteries and plots in Fig. 8 for the 16 anterior descent arteries. Those observations having a squared Mahalanobis distance above the 90% percentile of a chi-square with 2 degrees-of-freedom are considered to be outliers [16]. Outlying samples are not taken into account in the computation of the regression model and are highlighted with a circle in scattered plots.

There is a high correlation between manually and automatically computed PSR values for both arteries ($r \geq 86\%$). In
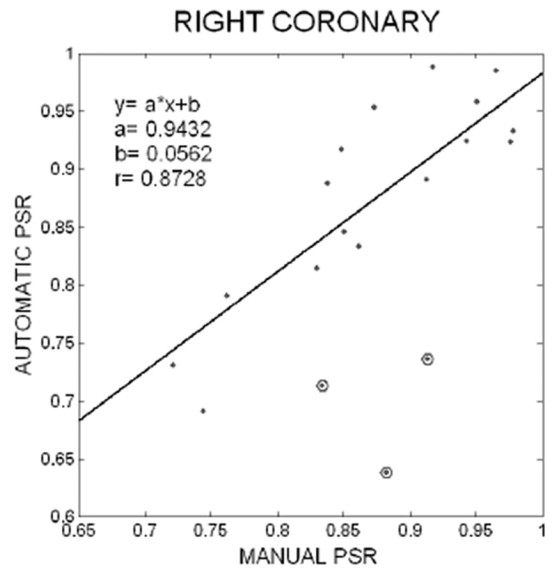

Fig. 7. Correlation between manual and automatically computed PSR for right coronary arteries.
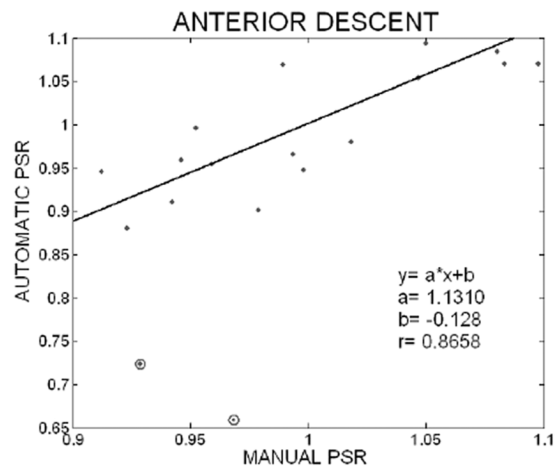

Fig. 8. Correlation between manual and automatically computed PSR for anterior descent arteries.

both cases, the regression lines are close to the identity, with $y = 0.9432x + 0.0562$ for the right coronary artery and $y = 1.1310x - 0.1280$ for the left anterior descending. Concerning outliers, they constitute less than 13% of the data analyzed and
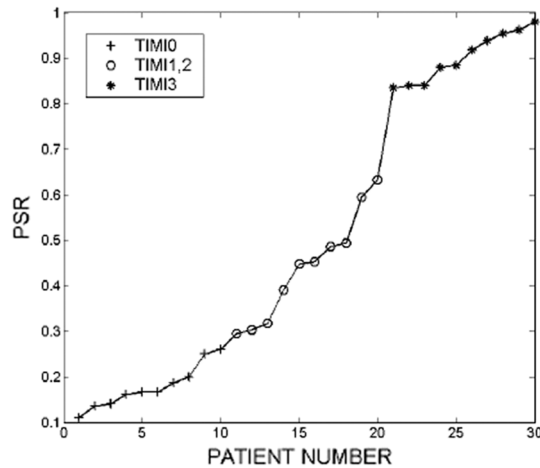
Fig. 9. Relation between TIMI flow and PSR.

mainly correspond to a substantial decrease in arterial points precision.

Regarding PSR reliability, the precision ranges are 84.71% $\pm$ 9.40% for the right coronary artery and 90.07% $\pm$ 13.00% for the left anterior descending. Nonarterial points included in the set used to compute $\mu(A)$ belong to the lower and higher percentiles of the distribution and, thus, do not significantly affect the value of PSR.

V. PSR APPLICABILITY

In order to illustrate PSR possibilities in clinical practice, we have computed PSR for patients presenting different degrees of arterial obstruction. Arterial flow is measured in terms of the thrombolysis in myocardial infarction (TIMI) grade [18]. The TIMI score is a discrete index with values of 0, 1, 2, and 3. A value of 0 indicates an infarcted artery, while 3 corresponds to a normal arterial flow. We have considered 30 patients with an infarcted right coronary artery and the following TIMI's: 10 patients with TIMI 0, 10 patients with TIMI's 1 and 2, and 10 patients with TIMI 3.

For each TIMI group, we have sorted the PSR values in order to see if there is any increasing dependency between the TIMI discrete index and the continuous PSR measure. Fig. 9 plots the TIMI value (x axis) against the sorted PSR (y axis). Values for TIMI 0 are represented with crosses, values for TIMI's 1, 2 with circles and values for TIMI 3 with asterisks. As expected, there is a monotonous increasing dependency between the TIMI grade and the value PSR. For TIMI's 0 and 3, we have a constant distribution with TIMI 0 PSR values significantly lower (with a PSR range 0.17 ± 0.05) than those attained for a normal flow (PSR within 0.86 ± 0.096). For TIMI 1, 2, the index PSR increasingly varies from TIMI 0 minimum to TIMI 3 maximum value.

In order to establish the relationship between TIMI scores and mean PSR values, we have performed two different one-tailed t-tests. The first null hypothesis states that the mean PSR value for TIMI 0 is greater than the mean value for TIMI's 1, 2; the second one states that the mean value for TIMI's 1, 2 is greater than the mean value for TIMI 3. Both of them were significant

($p = 1.7924e^{-6}$ and $p = 6.6214e^{-10}$, respectively) and, thus, the mean PSR values increase with the TIMI score.

VI. DISCUSSION AND CONCLUSION

This paper addresses objective automatic measurement of myocardial perfusion for the first time. On one hand, we present a two dimensional set of descriptors for contrast staining. The set of descriptors detects three main phenomena: myocardial staining, arterial staining and noise. On the other hand, we propose a measure of perfusion (the PSR index) in terms of the rate between arterial and myocardial staining intensities. Experiments address the assessment of the reliability of, both, extraction of the staining pattern and computation of the PSR index.

Assessment of the staining patterns concerns with the influence of noise and breathing. By the large interpatient variability, we have used supervised classification statistics on each patient to approach the former topics. Right coronary arteries without any observable lesion in the angiography have been used for the trial. Myocardial staining presents a precision and a recall over 95%, which indicates a high efficiency of the staining descriptors for myocardial staining characterization. The low rate of noisy pixels classified as myocardial (with a specificity in the noise class over 95%) shows their reliability. There is an increase in classification errors for the arterial class mainly due to a difficult manual labelling. In sequences at 12.5 frames per second arterial dynamics does not uniformly sweep its influence area but presents a jump-wise movement. This introduces background pixels in the arterial staining class. Besides only pixels swept by the right coronary and its main arteries are labelled as arterial class. This implies that capillaries and tiny branches (especially near the heart boundaries) are included in the background cluster. Still the arterial identification and precision rates are over 85.6%. We conclude that the proposed descriptors allow an objective extraction of the myocardial contrast dyeing.

Regarding breathing impact, we have compared classification errors for sequences obtained in apnea and with the patient normally breathing. The confidence intervals for the average difference between errors for the myocardial class show a bias towards sequences recorded in apnea. These sequences present a lower identification rate due to involuntary diaphragm movements. Therefore, we consider that the most sensible choice is recording sequences with the patient normally breathing.

Assessment of PSR addresses its application in clinical practice in terms of accuracy and reliability of automatically computed values. Accuracy has been determined by comparing PSR values computed with arterial points manually and automatically selected. Concerning reliability, automatic PSR values are faithful as far as the pixels used to compute the average arterial staining lye on the main coronary artery. We have checked such condition by computing the precision of the arterial points selected using the strategy described in Section V. The test set comprises 23 right coronary arteries and 16 left anterior descending arteries. There is a high correlation (over 86%) between manual and automatic PSR values except for 13% of the cases analyzed. Such cases are outlying values with an underestimated PSR due to aortic flash. For the remaining cases, the regression line is close to the line of identity for both coronary

arteries. Concerning PSR reliability, there are at most a 30% of nonarterial points involved in its computation. Since the intensity values of such points are within the distribution queues, they do not bias computations.

Concerning its real applicability possibilities, we have analyzed PSR values distribution for different degrees of epicardial flow. There is a monotonous dependence between manual TIMI grades and the continuous PSR measure. According to a preliminary study [19], such correlation also holds between PSR and the myocardial blush grade. This fact converts the proposed measure into a good candidate for a reliable quantification of myocardial perfusion.

A proper computation of staining patterns requires that any decrease in image grey-level (associated to the first Fourier frequency) occurs by contrast opacification. This is guaranteed if the acquisition protocol suits the following three requirements. First, the patient should be either in apnea or breath at least twice. Otherwise, breath movements might substantially modify the descriptors values. Second, and in the same fashion as MBA and TIMI assessment, we recommend exhausting the sequence acquisition time in order to ensure that the contrast agent is completely absorbed by the myocardium. Finally, it is also important that there is not panning of the patient table during the acquisition, so that the region of interest on the image corresponds to the same myocardium area along the sequence. Although the above points imply modifying the standard protocol, we consider that they do not represent a major inconvenience for a systematic and successful application in clinical practice.

REFERENCES

[1] G. Stone and M. Peterson *et al.*, "Impact of normalized myocardial perfusion after successful angioplasty in acute myocardial infarction," *J. Am. College Cardiol.*, vol. 39, no. 4, pp. 591–597, 2002.

[2] S. N. e. a. A. Kaltoff and M. Bottcher, "Sestamibi single photon emission computed tomography immediately after primary percutaneous coronary intervention identifies patients at risk for large infarcts," *Am. Heart J.*, vol. 151, no. 5, pp. 1108–1114, 2006.

[3] A. van't Hof and A. Liem *et al.*, "Angiographic assessment of myocardial reperfusion in patients treated with primary angioplasty for acute myocardial infarction: Myocardial blush grade," *Circulation*, vol. 97, pp. 2302–2306, 1998.

[4] M. Gibson, C. Cannon, and S. Murphy *et al.*, "Relationship of TIMI myocardial perfusion grade to mortality after administration of thrombolytic drugs," *Circulation*, vol. 101, pp. 125–130, 2000.

[5] A. Poli and R. Fetiveau *et al.*, "Integrated analysis of myocardial blush and st-segment elevation recovery after successful primary angioplasty real-time grading of microvascular reperfusion and prediction of early and late recovery of left ventricular function," *Circulation*, vol. 106, pp. 313–318, 2002.

[6] F. Bellandi and M. Leoncini *et al.*, "Markers of myocardial reperfusion as predictors of left ventricular function recovery in acute myocardial infarction treated with primary angioplasty," *Clin. Cardiol.*, vol. 27, no. 12, pp. 683–688, 2004.

[7] P. Haager and P. Christott *et al.*, "Prediction of clinical outcome after mechanical revascularization in acute myocardial infarction by markers of myocardial reperfusion," *J. Am. College Cardiol.*, vol. 41, no. 4, pp. 532–538, 2003.

[8] V. Bertomeu-González and V. Bodía *et al.*, "Limitations of myocardial blush grade in the evaluation of myocardial perfusion in patients with acute myocardial infarction and TIMI grade 3 flow," *Rev. Española Cardio.*, vol. 59, no. 6, pp. 575–581, 2006.

[9] S. Kaul, "Coronary angiography cannot be used to assess myocardial perfusion in patients undergoing reperfusion for acute myocardial infarction," *Heart*, vol. 86, pp. 483–484, 2001.

[10] C. Gibson, J. de Lemos, and S. Murphy *et al.*, "Methodologic and clinical validation of the TIMI myocardial perfusion grade in acute mi," *J. Thromb Thrombolysis*, vol. 14, pp. 233–237, 2002.

[11] A. Perez de Prado, F. Fernández-Vázquez, J. Cuellas-Ramón, and I. Iglesias-Garriz, "Coronary clearance frame count: A new index of microvascular perfusion," *J. Thromb Thrombolysis*, vol. 9, no. 2, pp. 97–100, 2005.

[12] C. Gibson and Schöming, "Angiographic assesment of both epicardial and myocardial perfusion," *Circulation*, vol. 109, pp. 3096–3105, 2004.

[13] A. V. Oppenheim and A. S. Willsky, *Signals & Systems*. Upper Saddle River, NJ: Prentice-Hall, 1997.

[14] R. Duda, P. Hart, and D. Stork, *Pattern Classification*. New York: Wiley, 2001.

[15] D. Gil, Discriminating myocardial blush in contrast angiography Computer Vision Center, Barcelona, Spain, Tech. Rep., 2006.

[16] P. J. Rousseeuw and A. M. Leroy, *Robust Regression and Outlier Detection*. New York: Wiley, 1987.

[17] S. Geisser, *Predictive Inference: An Introduction*. New York: Chapman Hall, 1993.

[18] T. S. Group, "The TIMI study group: The thrombolysis in myocardial infarction (TIMI) trial. Phase i findings," *New England J. Medicine*, vol. 312, pp. 932–936, 1985.

[19] O. Rodriguez-Leor, E. Nofrerias, and J. Mauri, "Perfusion ratio: A new tool to objectively assess microcirculation perfusion after primary percutaneous coronary intervention," presented at the ESC Congress 2006, Barcelona, Spain.